

Orientation-Robust Latent Motion Trajectory Learning for Annotation-free Cardiac Phase Detection in Fetal Echocardiography

Yingyu Yang^a, Qianye Yang^a, Can Peng^a, Elena D'Alberti^b, Olga Patey^b, Aris T. Papageorghiou^b, J. Alison Noble^a

^a*Institute of Biomedical Engineering, Department of Engineering Science, University of Oxford, Oxford, United Kingdom*

^b*Nuffield Department of Women's and Reproductive Health, University of Oxford, Oxford, United Kingdom*

Abstract

Fetal echocardiography is essential for detecting congenital heart disease (CHD), facilitating pregnancy management, optimized delivery planning, and timely postnatal interventions. Among standard imaging planes, the four-chamber (4CH) view provides comprehensive information for CHD diagnosis, where clinicians carefully inspect the end-diastolic (ED) and end-systolic (ES) phases to evaluate cardiac structure and motion. Automated detection of these cardiac phases is thus a critical component toward fully automated CHD analysis. Yet, in the absence of fetal electrocardiography (ECG), manual identification of ED and ES frames remains a labor-intensive bottleneck. We present ORBIT (Orientation-Robust Beat Inference from Trajectories), a self-supervised framework that identifies cardiac phases without manual annotations under various fetal heart orientation. ORBIT employs registration as self-supervision task and learns a latent motion trajectory of cardiac deformation, whose turning points capture transitions between cardiac relaxation and contraction, enabling accurate and orientation-robust localization of ED and ES frames across diverse fetal positions. Trained exclusively on normal fetal echocardiography videos, ORBIT achieves consistent performance on both normal (MAE = 1.9 frames for ED and 1.6 for ES) and CHD cases (MAE = 2.4 frames for ED and 2.1 for ES), outperforming existing annotation-free approaches constrained by fixed orientation assumptions. These results highlight the potential of ORBIT to facilitate robust cardiac phase detection directly from 4CH fetal echocardiography.

Keywords:

Cardiac phase detection, Self-supervised learning, Motion estimation, Fetal echocardiography

1. Introduction

Congenital heart disease (CHD) is one of the most common birth defects in the fetal population and remains a major global burden for child health [1]. Prenatal screening for CHD plays a critical role in reducing perinatal mortality, optimizing postnatal management, and supporting pregnancy planning [2]. Fetal echocardiography is an effective modality for detecting and evaluating CHD [3]. However, performing fetal echocardiography and accurately identifying CHD require intensive training in free-hand ultrasound and specialized expertise in fetal cardiology—factors that pose challenges for early CHD detection, particularly in low- and middle-income countries [4]. Therefore, improving the workflow for CHD detection in fetal echocardiography is of great importance [5]. Artificial intelli-

gence (AI) has shown strong potential in assisting fetal echocardiography analysis, including improving CHD detection rates [6, 7, 8, 9, 10, 11]. A fundamental step in echocardiography analysis is the identification of the end-diastole (ED) and end-systole (ES) frames, as these two key cardiac phases are critical for functional assessment and cardiac biometric measurements in both adult [12] and fetal echocardiography [13, 14, 15]. In practice, ED and ES correspond to the closure of the mitral and aortic valves, respectively [16]. When these valves are not clearly visible, surrogate parameters such as maximal and minimal ventricular volumes for ED and ES, respectively, can be used to define these phases [16].

Numerous automatic algorithms have been developed to detect ED/ES frames in adult [17, 18, 19] and fetal echocardiography [20, 21, 22, 23, 24]. However, these methods rely on training data with manual annotations, such as ED/ES indices or segmentation labels, limit-

*Preprint. Submitted to *Medical Image Analysis*.

ing their applicability in annotation-scarce settings. Although several unsupervised approaches have been proposed for adult echocardiography [25, 26, 27, 28], direct adaptation to fetal echocardiography remains challenging due to non-standardized imaging windows, variable fetal heart orientations, and potential fetal motion. Unlike adult 4-chamber (4CH) views, typically acquired from a fixed imaging angle, fetal 4CH echocardiography exhibits substantial orientation variability due to differences in fetal position. As illustrated in Figure 1, approximately 60% of our training data are apical 4CH views, while the remaining 40% consist of transverse or basal views. These challenges underscore the need for a unified model that can handle fetal heart orientation variability in fetal cardiac phase detection.

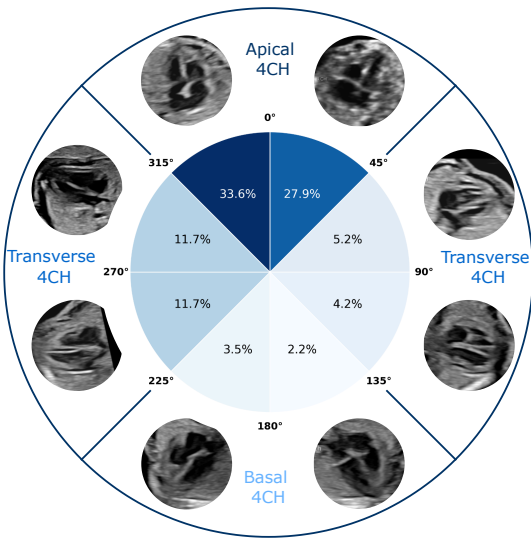


Figure 1: Orientation distribution in the training set. Fetal 4CH-view echocardiography exhibits greater orientation variability, primarily due to differences in fetal position and examination angle.

To overcome the challenges of orientation variability and the availability of annotations in fetal echocardiography, we propose ORBIT (Orientation-Robust Beat Inference from Trajectories), a novel self-supervised framework for fetal cardiac phase detection. ORBIT is annotation-free, orientation-robust, and effective across both normal and CHD cases.

The main contributions of this work are as follows:

- Annotation-free orientation-robust phase detection: We introduce a self-supervised method for identifying ED and ES frames in fetal 4CH echocardiography. The model learns a low-dimensional latent motion trajectory (1D/2D) that

captures cardiac relaxation and contraction directly from video data without any manual labels and is shown to generalize across diverse fetal heart orientations.

- Comprehensive evaluation of robustness: The model is trained solely on normal fetal echocardiography videos and evaluated across different orientation angles, CHD conditions, and preprocessing (cropping) strategies to assess both in- and out-of-distribution robustness.

This study builds upon our earlier work [29], which introduced an annotation-free framework for cardiac phase detection in adult and fetal apical 4CH views. In this extension, we make several key advances: (1) we replace the reconstruction-based self-supervision with a registration-based approach, introducing a new architecture for latent modeling of cardiac deformation that enhances robustness to varying heart orientations; (2) we double the number of normal videos used for in-distribution evaluation (88 vs. 44 in the previous work); (3) we conduct a detailed evaluation on 156 CHD videos to assess out-of-distribution robustness; and (4) we compare manual and tool-based cropping strategies to examine the preprocessing influence on self-supervised cardiac phase detection.

The remainder of this paper is organized as follows. Section 2 reviews related work on supervised and unsupervised cardiac phase detection and low-dimensional motion representation. Section 3 presents the ORBIT framework. Section 4 describes the dataset, implementation details, and experimental setup. Section 5 reports results on in-distribution and orientation performance as well as robustness to domain shifts (normal vs. CHD, manual vs. tool-based cropping). Finally, Section 6 concludes the paper.

2. Related work

2.1. Supervised cardiac phase detection in adult and fetal echocardiography

Supervised cardiac phase detection in 4CH echocardiography requires a large amount of annotated data, either through direct or indirect supervision. In adult echocardiography, direct approaches typically involve regressing the ED/ES frames directly from echocardiography inputs using neural networks, such as CNN-RNN frameworks [17, 22] or Vision Transformers [30], to estimate temporal ED/ES probabilities. Indirect approaches infer ED/ES timing from intermediate temporal predictions, such as left ventricular segmentation masks [31] or derived volume curves [19].

In fetal echocardiography, a hybrid object detection framework has been proposed to jointly perform standard plane recognition, cardiac cycle localization, and abnormal structure detection in both apical and basal four-chamber views [21]. An optimized pyramidal convolutional network with shuffle-attention has been developed for improved ED and ES detection, with separate models trained for apical, basal, and parasternal 4CH views [23]. More recently, long-term temporal dependencies and short-term motion cues have been jointly modeled by integrating optical flow with a Mamba U-Net architecture to regress frame-wise ED/ES probabilities in fetal echocardiography videos [24].

Although promising, supervised methods are fundamentally constrained by the amount of annotated data available for training. This limitation hinders their applicability in annotation-scarce settings, especially in fetal echocardiography, where large quantities of unlabelled video data are available but expert annotations are costly and time-consuming to obtain.

2.2. *Unsupervised cardiac phase detection in adult and fetal echocardiography*

Unsupervised methods for ED/ES detection aim to exploit the intrinsic periodicity of cardiac motion in 4CH echocardiography, without the help of explicit labels. Dimensionality-reduction techniques, such as locally linear embedding (LLE), have been used to project echocardiography videos onto a low-dimensional manifold, where cardiac phase transitions can be inferred through density analysis [25, 26]. However, these case-specific embeddings often lack interpretability and consistency when applied to larger datasets. Applying singular value decomposition (SVD) to spatio-temporal matrices derived from adult echocardiography videos has shown that the leading temporal singular vector can delineate cardiac phase transitions, although this analysis was demonstrated on a relatively small dataset of 20 cases [28]. Considering the inherently periodic nature of cardiac motion, circular latent representations have been explored using autoencoder-based frameworks, in which the cardiac cycle is constrained to follow a cyclic trajectory in latent space [32]. While the resulting latent representations exhibit semantic alignment with end-diastolic and end-systolic phases, these approaches do not explicitly predict their temporal locations. Related training-free unsupervised methods have modelled left ventricular expansion-contraction dynamics to identify ED/ES frames in adult echocardiography videos; although computationally efficient, such approaches typi-

cally require careful parameter tuning when transferred to new datasets [27].

Despite these advances, applications of unsupervised cardiac phase detection in fetal echocardiography remain limited. Our earlier work [29] proposed a self-supervised reconstruction-based framework called LMP (Latent Motion Profiling) with an interpretable latent subspace for studying cardiac phase dynamics, achieving promising ED/ES detection accuracy in both adult and fetal echocardiography. However, that method was restricted to apical 4CH views only and required manual orientation correction for other 4CH orientations, limiting its flexibility in handling fetal echocardiography data with diverse orientations. While orientation variability could, in principle, be mitigated by predicting heart orientation explicitly [33], our proposed method eliminates this requirement altogether. ORBIT does not rely on any prior orientation information, making it substantially more versatile and scalable for minimally annotated datasets.

2.3. *Low-dimensional representation in cardiac motion modelling*

Cardiac phase is closely linked to cardiac motion. However, cardiac motion is inherently high-dimensional and highly non-linear. Representing it in a low-dimensional space enables more efficient modeling and analysis. Approaches such as barycentric subspace projection [34] and polyaffine motion approximation [35, 36] have been proposed to capture complex cardiac dynamics while reducing computational complexity. Latent probabilistic deep learning models have also been employed to learn conditional motion from end-diastole to the entire cardiac cycle, facilitating scalability to larger datasets [37].

Inspired by these non-linear low-dimensional motion modeling strategies, we design our framework to learn a latent subspace representation from the temporal deformation field across the entire input video, enabling efficient and generalizable characterization of cardiac motion.

3. Methodology

Building on the insight that cardiac relaxation and contraction represent a global abstraction of highly complex heart motion, we hypothesize that a low-dimensional representation can capture cardiac phase information from high-dimensional deformation patterns. Therefore, we aim to learn the underlying deformation dynamics within an echocardiography video

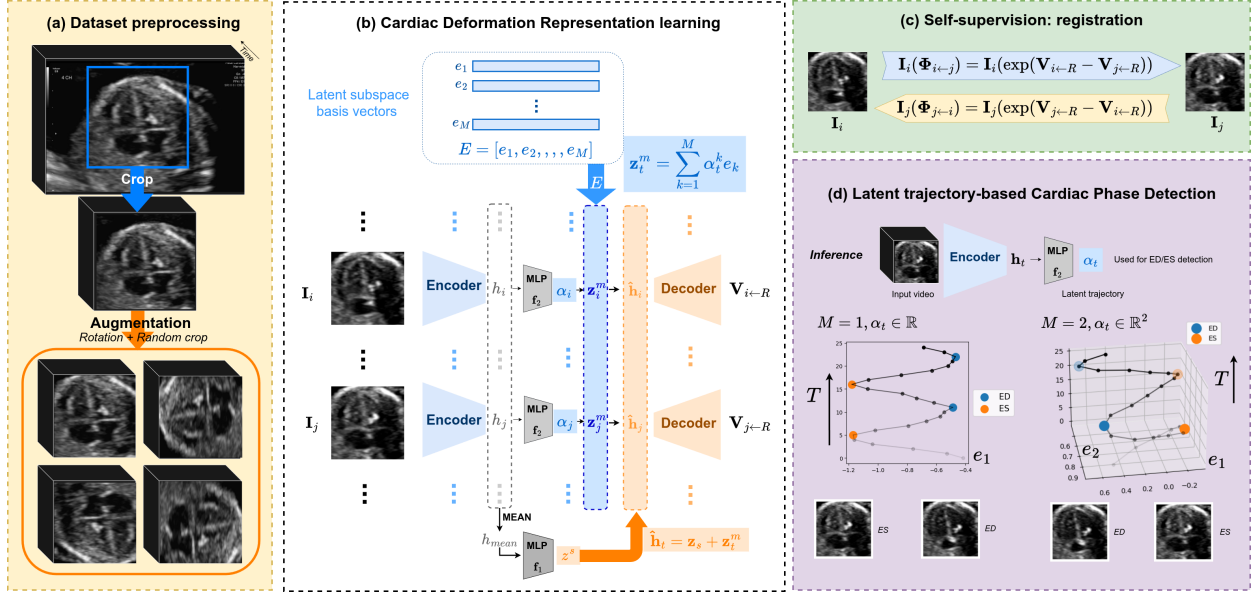


Figure 2: **Proposed ORBIT model for cardiac phase detection.** (a) Video preprocessing with heart area cropping and rotation augmentation (Section 4). (b) Latent decomposition for cardiac deformation representation learning (Section 3.2) and (c) its self-supervision aim via registration (Section 3.1). (d) Annotation-free cardiac phase detection from latent trajectory with latent subspace dimension $M = 1$ and $M = 2$ (Section 3.3).

and, through latent space decomposition, characterize cardiac phase transitions along a low-dimensional latent trajectory. In the following, we describe how to learn this latent trajectory via a self-supervised registration task and how cardiac phase can be consistently aligned with the resulting explainable trajectory, enabling robust ED/ES detection across fetal echocardiography videos with varying orientations.

3.1. Reference-Free Cardiac Deformation Estimation

Traditional cardiac deformation estimation methods typically require a reference frame, commonly the ED frame, to track motion relative to that frame [34, 35, 36, 37]. However, in our setting, the ED frame is unknown because it is the target of our detection task. Inspired by [38, 39], we introduce the concept of an abstract reference frame, which serves as a virtual bridge linking the deformation fields between any two arbitrary frames. Given a frame $\mathbf{I}_t : \mathbb{R}^2 \rightarrow \mathbb{R}^2$ from an echocardiography video, we use an autoencoder to estimate a deformation field $\Phi_{t \leftarrow R} : \mathbb{R}^2 \rightarrow \mathbb{R}^2$ that warps the current frame to the abstract reference frame R:

$$\hat{\mathbf{I}}_t = \mathbf{I}_t \circ \Phi_{t \leftarrow R} \approx R \quad (1)$$

Specifically, we consider a diffeomorphic deformation field parametrised by a stationary velocity field (SVF) $\mathbf{V}_{t \leftarrow R}$, such that $\Phi_{t \leftarrow R} = \exp(\mathbf{V}_{t \leftarrow R})$ [40].

Since the abstract reference frame R is unknown, direct supervision of registration is infeasible. Using a first-order approximation of the Baker–Campbell–Hausdorff formula [41], the deformation between any two arbitrary frames \mathbf{I}_i and \mathbf{I}_j can be approximated as:

$$\Phi_{j \leftarrow i} = \exp(\mathbf{V}_{j \leftarrow R} - \mathbf{V}_{i \leftarrow R}) \quad (2)$$

We can then deform \mathbf{I}_j according to this predicted deformation field to obtain $\hat{\mathbf{I}}_j = \mathbf{I}_j \circ \Phi_{j \leftarrow i}$, and train the network to make $\hat{\mathbf{I}}_j$ resemble \mathbf{I}_i using a normalized cross-correlation (NCC) similarity loss [42] (Equation 9).

3.2. Latent Trajectory Learning for Cardiac Deformation Representation

As stated above, given an echocardiography video $\mathbf{I} \in \mathbb{R}^{T \times H \times W}$, we train an autoencoder that predicts velocity fields $\mathbf{V} \in \mathbb{R}^{T \times 2 \times H \times W}$ between each frame and the abstract reference frame. The encoder $\mathcal{E} : \mathbb{R}^{H \times W} \rightarrow \mathbb{R}^D$ maps each frame to a latent vector $\mathbf{h}_t = \mathcal{E}(\mathbf{I}_t)$ of dimension D , while the decoder $\mathcal{D} : \mathbb{R}^D \rightarrow \mathbb{R}^{2 \times H \times W}$ reconstructs the frame-wise velocity field from a latent input $\hat{\mathbf{h}}_t$. The latent input to the decoder $\hat{\mathbf{h}}_t$ differs from the encoder output \mathbf{h}_t as shown in Figure 2(b). In order to capture the dynamics present in cardiac deformation, we model

$$\hat{\mathbf{h}}_t = \mathbf{z}^s + \mathbf{z}_t^m, \quad (3)$$

where \mathbf{z}^s denotes the static component, shared across all frames of the input video, i.e. serving as an anchor in the latent space. \mathbf{z}_t^m represents the motion component, capturing frame-specific deviations around this anchor. We constrain \mathbf{z}_t^m to a M -dimensional subspace of the latent space spanned by learnable orthogonal basis vectors

$$\mathbf{E} = [e_1, e_2, \dots, e_M] \in \mathbb{R}^{M \times D}, M \ll D, \quad (4)$$

which are optimized jointly with the network parameters using Gram-Schmidt orthonormalization [39]. Two 2-layer multilayer perceptrons (MLPs) $\mathbf{f}_1 : \mathbb{R}^D \rightarrow \mathbb{R}^D$ and $\mathbf{f}_2 : \mathbb{R}^D \rightarrow \mathbb{R}^M$, are used to obtain the latent components respectively from encoder output \mathbf{h}_t :

$$\mathbf{z}^s = \mathbf{f}_1\left(\frac{1}{T} \sum_{t=1}^T \mathbf{h}_t\right) \quad (5)$$

$$\mathbf{z}_t^m = \mathbf{E}^\top \alpha_t \quad (6)$$

Specifically, we denote the output of \mathbf{f}_2 as:

$$\alpha_t = \mathbf{f}_2(\mathbf{h}_t), \quad (7)$$

representing the coordinates of each motion component in the low-dimensional subspace. We obtain the frame-wise velocity field from the decoder:

$$\mathbf{V}_{t \leftarrow R} = \mathcal{D}(\hat{\mathbf{h}}_t) = \mathcal{D}(\mathbf{z}^s + \mathbf{z}_t^m) \quad (8)$$

To train the model, we define the registration loss at the video level. Applying Equation 2, each frame is registered to up to five subsequent frames:

$$\mathcal{L} = - \sum_{f=1}^5 \sum_{t=1}^{T-f} (NCC(\mathbf{I}_t \circ \Phi_{t \leftarrow t+f}, \mathbf{I}_{t+f}) + NCC(\mathbf{I}_{t+f} \circ \Phi_{t+f \leftarrow t}, \mathbf{I}_t)) \quad (9)$$

This encourages temporal consistency and smooth deformation dynamics across cardiac cycles.

3.3. Orientation-Robust Latent Trajectory-Based Cardiac Phase Detection

After training, only the encoder is required to analyze cardiac phase dynamics. Each video is represented by a sequence of latent coordinates $\{\alpha_t, t = 1, \dots, T\}$, which form a low-dimensional trajectory that characterizes periodic cardiac motion over time. We restrict the latent motion dimension to very low number ($M = 1$ and $M = 2$) and analyze the latent trajectory to identify cardiac phase transitions without any manual annotation. Figure 2(d) illustrates representative examples of 1D and 2D latent trajectories, where the turning points correspond to ED and ES. The specific association of

ED and ES with individual turning points is determined based on the observed contraction and relaxation patterns in the corresponding four-chamber (4CH) videos on the validation set. We detect turning points by locating peaks and valleys in the latent trajectory using the `find_peaks` function from `scipy` [43]. For model with $M = 2$, we select one direction to form a 1D trajectory and perform peak and valley detection.

4. Experiments and settings

4.1. Datasets

In this study, we curated a dataset of 4CH view B-mode echocardiography videos acquired during the second trimester of gestation at the John Radcliffe Hospital, Oxford University Hospitals NHS Foundation Trust, UK. All videos were obtained using GE Voluson E10 and E8 ultrasound systems, with a frame resolution of 1136×786 pixels. The dataset forms part of a retrospective cohort collected under the CAIFE study, which aims to develop artificial intelligence (AI) models for the early detection of congenital heart disease (CHD) from ultrasound videos [5].

- **Training and validation sets:** The training and validation sets comprise 422 videos from 273 healthy participants, each contributing between 1 and 4 videos. The data were split into 85% for training and 15% for validation, setting the same configuration for all models presented in this study. No ED or ES annotations are available for either the training or validation sets.
- **Normal test set:** The normal test set consists of 88 videos from 78 non-overlapping healthy participants, with 1–2 videos per participant. Frame rates range from 47 to 81 Hz, with a mean of 68 Hz. One experienced fetal cardiologist and one obstetrician with expertise in fetal cardiology independently annotated the ED and ES frames, resulting in a total of 317 annotated frames.
- **Abnormal test set:** The abnormal test set includes 156 videos from 47 participants diagnosed with congenital heart disease (CHD), covering 13 distinct CHD conditions. Each participant contributed between 1 and 8 videos. Frame rates range from 30 to 87 Hz, with a mean of 48 Hz. The same operators independently annotated the ED and ES frames for these CHD cases, yielding a total of 531 annotated frames. A detailed breakdown of video counts by CHD condition is provided in Table 1,

and the distribution of frame rates for both normal and abnormal test sets is illustrated in Figure 3.

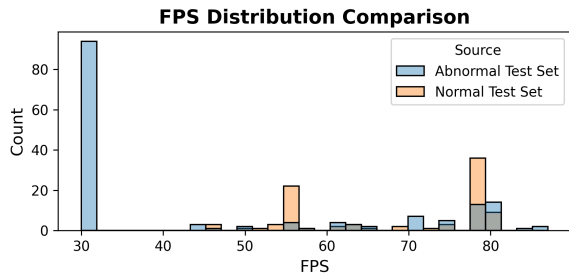


Figure 3: **Histogram of frames-per-second (FPS) distributions for normal and abnormal test videos.** Blue and orange bars correspond to abnormal and normal cases, respectively; overlapping bins are shown in gray.

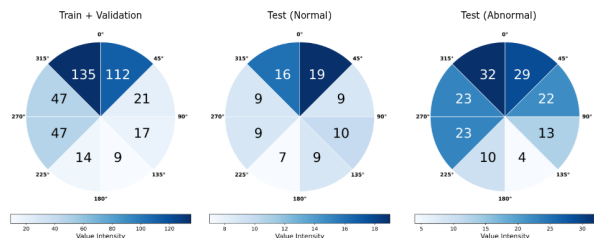


Figure 4: **Orientation distribution** in train/validation set (normal), test (normal) set and test (abnormal) set.

Orientation distribution: An experienced engineer manually annotated the orientation of each video by assigning it to one of eight predefined angle groups, as illustrated in Figure 1. Figure 4 shows the distribution of heart orientations at the video level for the training/validation, normal test, and abnormal test sets, respectively.

4.2. Implementation

For the training and validation sets, the heart region was manually cropped and resized to 156×156 pixels, with a temporal downsampling factor of 2 for data preparation. During training, 25 consecutive frames were randomly selected, and a consistent 128×128 region was randomly cropped from each video clip as model input. To augment the data, each video was additionally rotated four times clockwise by 0° (original), 90° , 180° , and 270° . The model was trained using the Adam optimizer with a learning rate of $1e-4$, a batch size of 16, and for 500 epochs. The localized NCC loss was set with a window size of 9. We

Split	Diagnosis	#Participant	#Videos
Train/Validation	Normal	273	422
Test	Normal	78	88
	CHD	47	156
	VSD	11	39
	CAVSD/B	10	41
	HLHS	4	17
	COA	4	7
	MA/VSD	4	6
	CAUSD/U	3	13
	TAVSD/NRA	3	10
	TAPVC/IC	2	9
	PA/IVS	2	7
	DTV	1	4
	FA/T	1	1
	ILA	1	1
	UVH/RAI	1	1

Table 1: **Video statistics.** Detailed explanation of CHD abbreviation are presented in Appendix A.

used the same model architecture as the baseline model LMP [29]¹, with appropriate output reformulation to fit in self-supervised registration as described in Section 3. The model with the lowest validation loss during training was selected for subsequent evaluation. For evaluation on the test sets, the heart region was manually cropped and each video was resized to 128×128 pixels without temporal downsampling.

4.3. Evaluation metrics

We follow previous work on cardiac phase detection evaluation using the mean absolute error (MAE) between each predicted ED or ES frame and the corresponding ground-truth frames annotated by expert cardiologists [17, 21, 24]. Since multiple ED/ES events occur in each video, the error for each ground-truth frame is computed with respect to its nearest predicted frame. To account for variability in frame rate (frames per second, fps) and heart rate (beats per minute, bpm) across the test videos, we additionally report MAE in milliseconds (MAE-ms) and MAE as a percentage of the cardiac cycle (MAE-%cycle). In addition, we quantify the detection success rate by applying a 50% threshold to the MAE-%cycle metric, representing the proportion of confidently matched ED/ES events.

4.4. Statistical analysis

Because cardiac cycles within the same video are highly correlated, the assumption of independence does

¹Model architecture details can be found in the project repository <https://github.com/YingyuYyy/CardiacPhase>.

Method	Annotator	MAE (frames)		MAE (ms)		MAE (% cycle)		% Samples	
		mean (std)		mean (std)		mean (std)		MAE/cycle < 50	
		ED	ES	ED	ES	ED	ES	ED	ES
Inter-Observer	#1 vs #2	1.6 (1.4)	1.0 (1.1)	23.8 (20.4)	14.9 (15.5)	6.0 (5.2)	3.8 (4.0)	100.0	100.0
LMP [29]	#1	3.4 (6.7)	3.7 (7.3)	51.1 (102.3)	56.4 (107.2)	12.9 (26.1)	14.3 (27.4)	93.4	93.1
	#2	3.8 (6.6)	3.4 (7.4)	58.5 (100.6)	52.1 (109.0)	14.7 (25.7)	13.1 (27.2)	92.4	92.7
ORBIT (ours)	#1	1.9 (3.6)**	1.6 (2.6)***	28.2 (53.0)**	23.5 (41.7)***	7.2 (13.8)**	6.0 (10.8)***	98.0	98.7
	#2	2.4 (3.4)**	1.5 (2.5)***	35.7 (49.0)**	22.5 (39.9)***	9.0 (12.4)**	5.6 (10.2)***	97.8	98.7

Table 2: **Cardiac phase detection in fetal echocardiography (88 normal videos).** Statistical test performed between ORBIT and LMP. ** $p < 0.01$, *** $p < 0.001$.

not hold for event-level analyses (ED or ES). Moreover, each participant may contribute multiple videos acquired under similar anatomical or imaging conditions, making video-level or cycle-level paired testing inappropriate. To address these dependencies, participant-level aggregation is used for non-parametric group comparisons, treating each participant as an independent observational unit. We employ linear mixed-effects models to evaluate statistical significance while leveraging all available data. In these models, the error metric is specified as the dependent variable, method or group are modeled as fixed effects, and random intercepts are included for participant and video to account for intra-participant and intra-video variability.

4.5. Experiments

We perform the following experiments to demonstrate the effectiveness and robustness of the proposed ORBIT method.

4.5.1. In-distribution experiments

In-distribution evaluations are conducted on normal test cases. First, we compared our approach with LMP [29] ($M = 2$), which requires manual orientation correction toward the apical direction before being fed into the deep learning model. In contrast, our method operates without any prior knowledge of heart orientation.

Second, to ensure a fair comparison, we retrained the LMP model without manual orientation correction but following the same training strategy as our method, i.e., by randomly rotating the training data to enable learning of the underlying cardiac phase and to assess performance under unknown orientations. Both methods were compared using their 1D latent motion subspace representations for the ease of visualization (we observed the same trend with models of 2D models.)

4.5.2. Out-of-distribution experiments

Since the model was trained entirely on normal fetal echocardiography videos, we investigated its robustness under distributional shift—specifically, its performance on cases with congenital heart disease conditions. Additionally, we tested the influence of an automatic heart cropping tool [44] for video preprocessing. Because the region of interest (ROI) was automatically detected using a deep learning-based cropping tool, which can occasionally mislocalize the heart (e.g., incomplete, oversized, or undersized crops), we further evaluated robustness by comparing performance between automatically and manually cropped frames.

5. Results

5.1. In-distribution results

5.1.1. Performance on Normal Test Data

Table 2 presents the evaluation results on the normal test videos. The proposed ORBIT framework consistently and significantly outperforms the baseline method LMP in detecting both ED and ES events, measured by MAE in frames, milliseconds, and percentage of the cardiac cycle. In particular, ORBIT reduces the mean error in cycle percentage by 5% for ED and 7% for ES, achieving prediction accuracy closer to inter-observer variability. Moreover, ORBIT does not rely on any orientation information for cardiac phase prediction, making it substantially more versatile than the baseline LMP model, which requires manual rotation of input videos toward the apical orientation.

5.1.2. Orientation Robustness

The key improvement of ORBIT lies in its orientation robustness — it detects cardiac phase consistently across heart orientations, unlike the baseline model LMP. We define orientation robustness in unsupervised cardiac phase detection as the ability of detecting

Self-supervision	Annotator	MAE (frames)		MAE (ms)		MAE (% cycle)		% Samples	
		mean (std)		mean (std)		mean (std)		MAE/cycle < 50	
		ED	ES	ED	ES	ED	ES	ED	ES
Inter-Observer	#1 vs #2	0.8 (1.0)	0.8 (1.0)	16.9 (20.8)	19.2 (22.5)	4.2 (5.1)	4.8 (6.0)	100.0	100.0
LMP [29]	#1	3.3 (6.8)	3.3 (7.1)	74.2 (133.8)	74.3 (140.0)	18.4 (33.4)	18.0 (32.9)	90.2	89.8
	#2	3.5 (6.7)	3.2 (7.1)	78.6 (132.0)	70.6 (138.6)	19.8 (34.1)	17.4 (33.5)	90.8	89.0
ORBIT (ours)	#1	2.4 (3.6)**	2.1 (3.8)***	56.0 (75.0)	47.3 (81.6)*	13.9 (19.0)*	11.8 (20.7)**	95.3	95.3
	#2	2.5 (3.6)**	2.0 (3.8)***	59.5 (77.5)	48.1 (82.3)*	14.9 (19.8)*	12.2 (21.4)**	94.7	95.3

Table 3: **Cardiac phase detection in fetal echocardiography (156 CHD videos).** Statistical test performed between ORBIT and LMP. * $p < 0.05$, ** $p < 0.01$, *** $p < 0.001$.

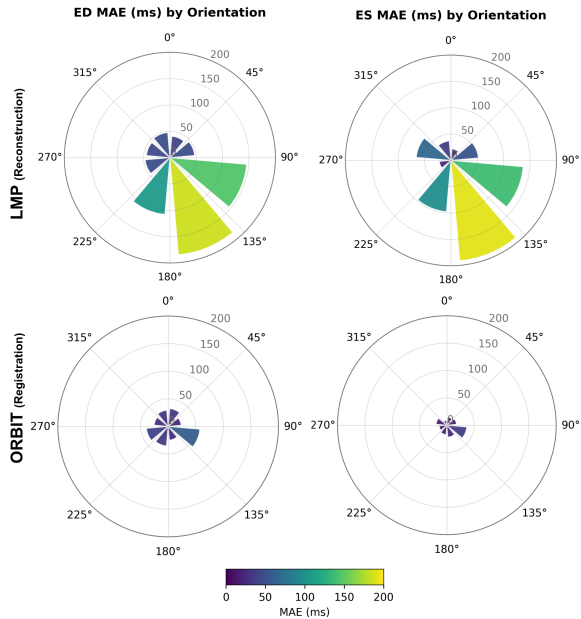


Figure 5: **Cardiac phase detection MAE (ms) grouped by orientation** using LMP (reconstruction self-supervision) and our ORBIT (deformation self-supervision) respectively.

systole and diastole consistently using the learned latent trajectory, regardless of input orientation. In other words, the model can infer cardiac phase without interpreting the trajectory based on the heart angle of the input video.

Both LMP and ORBIT employ latent motion trajectory modeling, but they differ fundamentally in what the trajectory represents. LMP learns the trajectory of echocardiographic appearance through image reconstruction, whereas ORBIT learns the trajectory of cardiac deformation through image registration.

As shown in Figure 5, the latent trajectory learned by LMP exhibits strong orientation dependency — errors between 90° and 225° increase remarkably for both ED and ES. In contrast, ORBIT maintains a nearly flat

error distribution across all orientations, demonstrating robustness.

We illustrate an example in Figure 7: when visualizing the 1D latent trajectories for one validation case under four orientations, LMP produces an inverted trajectory at one orientation (in red), effectively swapping the meanings of ED and ES. This inversion indicates that reconstruction-based models like LMP require explicit orientation information to interpret phase correctly. ORBIT, however, yields consistent trajectories across all orientations, reflecting true orientation invariance.

To investigate the reason for this robustness, we visualized the static component \mathbf{z}^s using Isomap dimensionality reduction on the validation set (Figure 6). The reconstruction-based model (LMP) shows mixed embeddings across orientation groups, while the registration-based ORBIT produces manifolds where static components are naturally grouped by orientation. This disentanglement removes the influence of heart orientation, allowing the latent motion component to capture a stable and consistent motion pattern that is explainable at group level, resulting in orientation-robust phase detection.

5.2. Out-of-distribution results

5.2.1. Performance on Abnormal Test Data

Table 3 summarizes the overall cardiac phase detection errors on abnormal (CHD) test data for both the baseline LMP model and the proposed ORBIT model. Consistent with the normal-case results, ORBIT achieves lower mean absolute errors (MAE) in both frames and cardiac-cycle percentage compared with LMP.

To further assess robustness across physiological conditions, we compared the participant-level MAE (median/mean of error in frames) between normal and abnormal groups for each method and each phase using the Mann–Whitney U test. The differences between groups were not statistically significant ($p > 0.05$ for

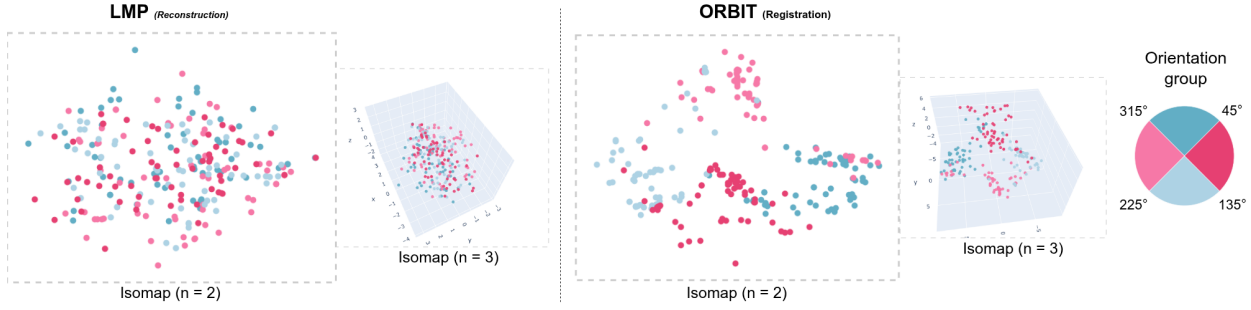


Figure 6: Isomap dimension reduction visualization of the static component z^s on validation dataset (63 videos * 4 rotations).

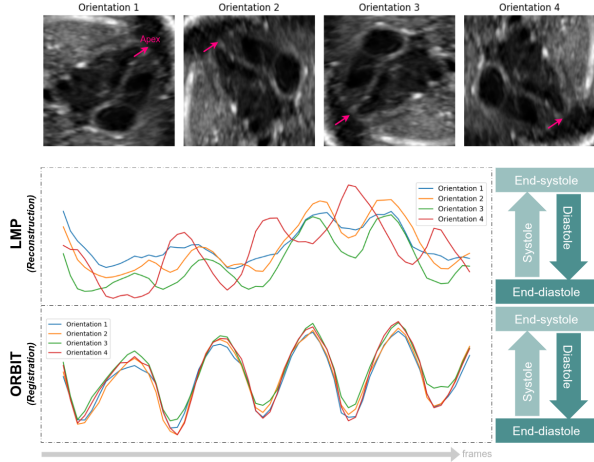


Figure 7: Latent motion curve (1D) consistency across orientations. Four orientations of the same video are shown in the first row, with red arrows indicating the apex location. The second row shows 1D latent trajectories from the LMP encoder, where one trajectory (red) exhibits an inverted trend. The third row shows ORBIT trajectories, which are consistent across orientations.

both median and mean) for either LMP or ORBIT, indicating that both latent-trajectory models maintain comparable accuracy on abnormal fetal hearts.

A modest degradation is observed when errors are expressed in milliseconds or cardiac-cycle percentage on the abnormal test set. This likely reflects acquisition characteristics: the abnormal dataset is captured at a lower frame rate (Figure 3), with many cases recorded at 30 fps. Because time-based metrics scale with frame interval, lower fps leads to larger apparent temporal errors. This discrepancy arises from retrospective data storage practices, where high-frame-rate acquisitions are often down-sampled to 30 fps to reduce file size.

Although the overall degradation in mean absolute error (MAE) for abnormal cases is not statistically significant at the group level, we are interested whether ORBIT’s performance varies across different CHD sub-

Group	MAE (frames)		MAE (% cycles)	
	mean (std)		ED	ES
	ED	ES	ED	ES
Normal	2.4 (3.4)	1.5 (2.5)	9.0 (12.4)	5.6 (10.2)
CHD	2.5 (3.6)	2.0 (3.8)	14.9 (19.8)	12.2 (21.4)
VSD	1.6 (2.5)	1.6 (3.4)	9.1 (12.4)	9.0 (16.4)
CAVSD/B	3.0 (3.7)*	1.8 (3.1)	16.9 (21.7)*	9.9 (17.1)
HLHS	3.9 (6.7)	3.0 (5.7)*	20.9 (26.8)*	20.5 (33.6)***
COA	2.1 (1.0)	2.0 (3.9)	7.8 (3.3)	7.5 (12.6)
MA/VSD	2.0 (2.0)	1.2 (1.2)	14.7 (16.6)	7.5 (8.8)

Table 4: Evaluation between normal and different CHD conditions using ORBIT method. (#2 Annotator). Statistical comparison performed between Normal group and each CHD condition group. * $p < 0.05$, ** $p < 0.01$, *** $p < 0.001$.

types. Table 4 reports the cycle-level MAE (in frames) for several CHD conditions. For statistical reliability, we analyze only CHD categories with at least four participants (see Table 1).

Across specific CHD conditions, the model demonstrates stable performance in VSD, COA, and MA/VSD groups, with MAE values similar to those in the normal cohort. In contrast, larger deviations are observed in CAVSD/B and HLHS cases, where errors increase notably for ED prediction in CAVSD/B (16.9% vs. 9.0%) and for both ED and ES predictions in HLHS (20.9% and 20.5% of the cardiac cycle, respectively). These differences can be attributed to underlying anatomical and motion characteristics. VSD and mild forms of COA typically preserve biventricular structure and global contraction patterns similar to those seen in normal hearts, enabling ORBIT to generalize effectively from normal training data and maintain consistent ED/ES detection accuracy. In contrast, CAVSD/B and HLHS are characterized by severely altered ventricular morphology and atypical motion dynamics, which may reduce the salience of the deformation cues that ORBIT relies on to extract latent motion trajectories. As a result, ED

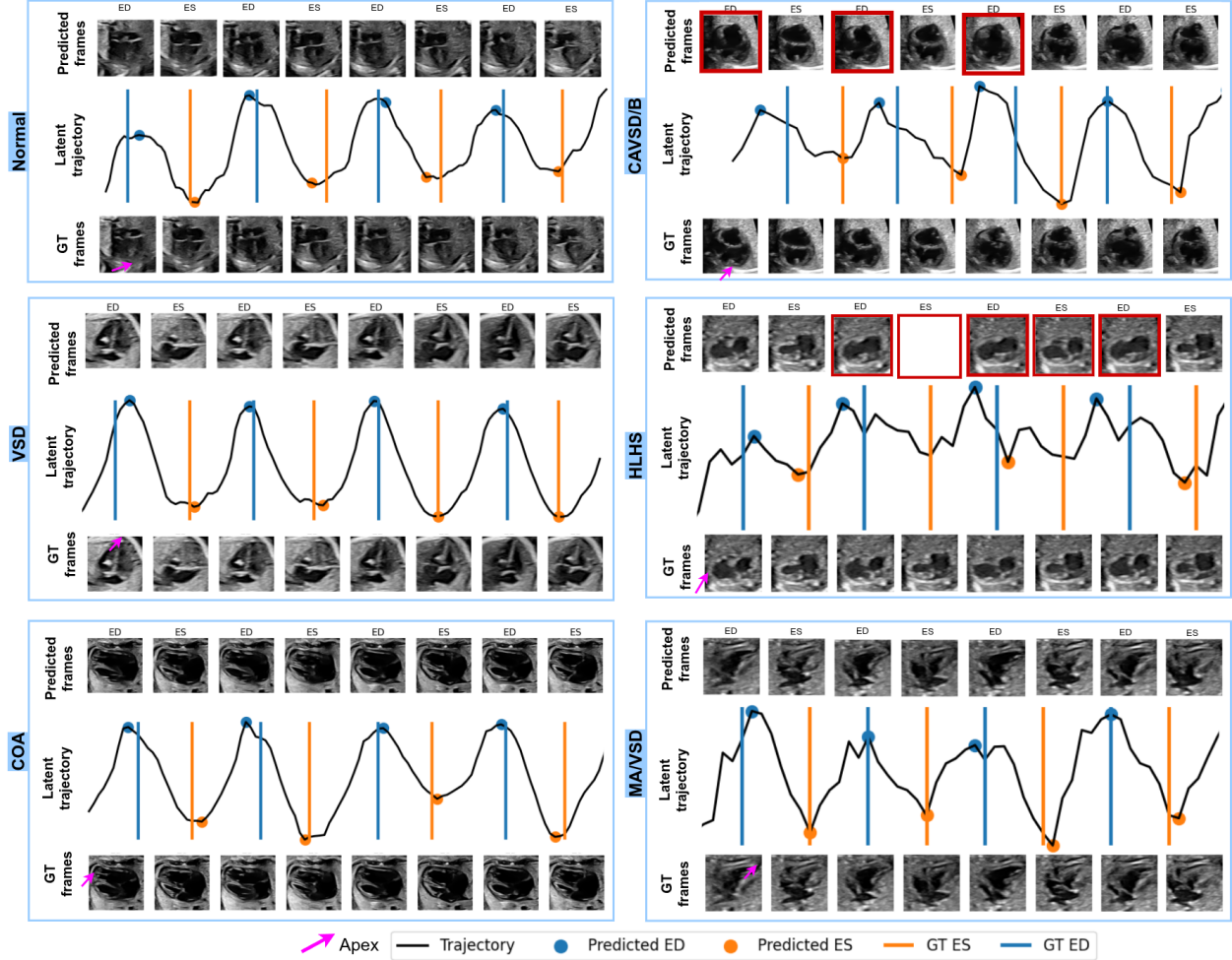


Figure 8: **Prediction examples using ORBIT.** Red box indicates MAE larger than 2 frames.

and ES turning points become less well defined in the latent space, leading to increased prediction error. Representative one-dimensional latent trajectory examples are shown in Fig. 8.

Together, these results suggest that while ORBIT performs robustly across most CHD morphologies. Prediction accuracy decreases for cases with complex ventricular morphology and dysfunction, particularly affecting ED frame prediction.

5.2.2. Effect of Cropping Variations

To assess robustness to preprocessing differences, we compared performance between manually cropped and automatically (tool-based) cropped images using the FEHT method [44], as summarized in Table 5. For both LMP and ORBIT, automatic cropping increased the mean error by approximately one frame on the abnor-

Method	Crop Strategy	MAE (frames)	
		mean (std)	
		ED	ES
LMP [29]	Manual	3.5 (6.7)	3.2 (7.1)
	FEHT [44]	4.4 (6.8)***	4.0 (7.2)***
ORBIT (ours)	Manual	2.5 (3.6)	2.0 (3.8)
	FEHT [44]	3.5 (4.9)***	3.0 (4.9)***

Table 5: **Evaluation on abnormal test data under different cropping strategies (#2 Annotator).** Statistical comparison performed between crop strategies for each method. Stars: * $p < 0.05$, ** $p < 0.01$, *** $p < 0.001$.

mal test set. This degradation is primarily attributed to imperfect alignment of the automatically extracted heart region with the manually defined region used during training. The results highlight that consistent and ac-

curate localization of the cardiac region remains critical for reliable phase inference in latent-trajectory-based methods. Because ORBIT relies on capturing subtle motion patterns within the heart region, the cropped area should have sufficient resolution and minimal background interference.

6. Discussion and Conclusion

In this work, we proposed ORBIT (Orientation-Robust Beat Inference from Trajectories), a novel self-supervised framework for fetal cardiac phase detection that operates without manual annotations and is robust to arbitrary heart orientations in four-chamber fetal echocardiography videos. ORBIT learns to decompose stationary velocity fields that parameterize the deformation of each input video sequence. The resulting latent motion component forms a one-dimensional trajectory that encodes cardiac contraction and relaxation as a cyclical back-and-forth motion, from which ED and ES frames can be efficiently inferred without supervision. Trained solely on normal fetal echocardiography videos, ORBIT demonstrates consistent performance on both normal and abnormal (CHD) data, without requiring any orientation information. This orientation robustness distinguishes ORBIT from previous latent trajectory-based methods, which rely on explicit orientation alignment. The strong and consistent performance across diverse orientations underscores its potential as a foundational component for real-world fetal video analysis, including heart beat segmentation, video summarization, and other downstream tasks in fetal echocardiography interpretation. Disease-wise evaluation further revealed that ORBIT maintains stable accuracy across most common CHD types, while showing increased sensitivity in certain severe cases. Although limited sample sizes of CHD cases prevent definitive conclusions, these findings suggest that latent motion trajectory modeling may be used for capturing disease-specific motion signatures. Future work will investigate this direction to explore the potential of ORBIT for prenatal congenital heart disease characterization and detection.

Appendix A. Congenital heart diseases included in our study

We present the full description of each congenital heart disease included in our study in Table A.6.

Abbreviation	Full name
CAVSD/B	Complete atrioventricular septal defect with balanced ventricles
CAVSD/U	Complete atrioventricular septal defect with unbalanced ventricles
COA	Coarctation of the aorta
DTV	Dysplastic tricuspid valve
FA/T	Fetal Arrhythmias/Tachycardia
HLHS	Hypoplastic left heart syndrome
ILA	Isolated left isomerism
MA/VSD	Mitral atresia with ventricular septal defect
PA/IVS	Pulmonary atresia with the intact interventricular septum
TAPVC/IC	Total anomalous pulmonary venous connections (infra-cardiac type)
TAWSD/NRA	Tricuspid atresia with ventricular septal defects and normally related great arteries (NRA)
UVH/RAI	Univentricular heart with right atrial isomerism (RAI)
VSD	Moderate/large ventricular septal defects

Table A.6: CHD condition names.

Acknowledgement

This work was supported by the InnoHK-funded Hong Kong Centre for Cerebro-cardiovascular Health Engineering (COCHE) Project 2.1 (Cardiovascular risks in early life and fetal echocardiography) and partly supported by the UKRI grant EP/X040186/1 (Turing AI Fellowship). Co-authors J. Alison Noble and Aris Papageorghiou were supported by the Oxford Partnership Comprehensive Biomedical Research Centre with funding from the NIHR Biomedical Research Centre (BRC) funding scheme.

References

[1] M. S. Zimmerman, A. G. C. Smith, C. A. Sable, M. M. Echko, L. B. Wilner, H. E. Olsen, H. T. Atabay, A. Awasthi, Z. A. Bhutta, J. L. Boucher, et al., Global, regional, and national burden of congenital heart disease, 1990–2017: a systematic analysis for the global burden of disease study 2017, *The Lancet Child & Adolescent Health* 4 (2020) 185–200.

[2] L. E. Hunter, J. M. Simpson, Prenatal screening for structural congenital heart disease, *Nature Reviews Cardiology* 11 (2014) 323–334.

[3] M. T. Donofrio, A. J. Moon-Grady, L. K. Hornberger, J. A. Copel, M. S. Sklansky, A. Abuhamad, B. F. Cuneo, J. C. Huhta, R. A. Jonas, A. Krishnan, et al., Diagnosis and treatment of fetal cardiac disease: a scientific statement from the american heart association, *Circulation* 129 (2014) 2183–2242.

[4] L. Zühlke, J. Lawrenson, G. Comitis, R. De Decker, A. Brooks, B. Fourie, L. Swanson, C. Hugo-Hamman, Congenital heart disease in low-and lower-middle-income countries: current status and new opportunities, *Current cardiology reports* 21 (2019) 163.

[5] O. Patey, N. Hernandez-Cruz, E. D’Alberti, B. Šalović, J. A. Noble, A. T. Papageorghiou, Prenatal detection of congenital heart defects using the deep learning-based image and video analysis: protocol for clinical artificial intelligence in fetal echocardiography (caife), an international multicentre multidisciplinary study, *BMJ open* 15 (2025) e101263.

[6] D. Mishra, M. Salehi, P. Saha, O. Patey, A. T. Papageorghiou, Y. M. Asano, A. Noble, Self-supervised learning of echocardiographic video representations via online cluster distillation, in: *The Thirty-ninth Annual Conference on Neural Information Processing Systems*, 2025.

[7] E. D’Alberti, O. Patey, C. Smith, B. Šalović, N. Hernandez-Cruz, J. A. Noble, A. T. Papageorghiou, Artificial intelligence-enabled prenatal ultrasound for the detection of fetal cardiac abnormalities: a systematic review and meta-analysis, *eClinicalMedicine* (2025).

[8] M. M. K. Sarker, V. K. Singh, M. Alsharid, N. Hernandez-Cruz, A. T. Papageorghiou, J. A. Noble, Comformer: Classification of maternal-fetal and brain anatomy using a residual cross-covariance attention guided transformer in ultrasound, *IEEE Transactions on Ultrasonics, Ferroelectrics, and Frequency Control* 70 (2023) 1417–1427.

[9] R. Arnaout, L. Curran, Y. Zhao, J. C. Levine, E. Chinn, A. J. Moon-Grady, An ensemble of neu-

ral networks provides expert-level prenatal detection of complex congenital heart disease, *Nature medicine* 27 (2021) 882–891.

[10] C. P. Bridge, C. Ioannou, J. A. Noble, Automated annotation and quantitative description of ultrasound videos of the fetal heart, *Medical image analysis* 36 (2017) 147–161.

[11] M. A. Maraci, C. P. Bridge, R. Napolitano, A. Papegeorgiou, J. A. Noble, A framework for analysis of linear ultrasound videos to detect fetal presentation and heartbeat, *Medical image analysis* 37 (2017) 22–36.

[12] R. M. Lang, L. P. Badano, V. Mor-Avi, J. Afilalo, A. Armstrong, L. Ernande, F. A. Flachskampf, E. Foster, S. A. Goldstein, T. Kuznetsova, et al., Recommendations for cardiac chamber quantification by echocardiography in adults: an update from the american society of echocardiography and the european association of cardiovascular imaging, *European Heart Journal-Cardiovascular Imaging* 16 (2015) 233–271.

[13] J. Carvalho, R. Axt-Fliedner, R. Chaoui, J. Copel, B. Cuneo, D. Goff, L. Gordin Kopylov, K. Hecher, W. Lee, A. Moon-Grady, et al., Isuog practice guidelines (updated): fetal cardiac screening., *Ultrasound Obstet Gynecol* 61 (2023) 788–803.

[14] A. J. Moon-Grady, M. T. Donofrio, S. Gelehrter, L. Hornberger, J. Kreeger, W. Lee, E. Michelfelder, S. A. Morris, S. Peyvandi, N. M. Pinto, et al., Guidelines and recommendations for performance of the fetal echocardiogram: an update from the american society of echocardiography, *Journal of the American Society of Echocardiography* 36 (2023) 679–723.

[15] F. Crispí, B. Valenzuela-Alcaraz, M. Cruz-Lemini, E. Gratacós, Ultrasound assessment of fetal cardiac function, *Australasian journal of ultrasound in medicine* 16 (2013) 158–167.

[16] R. O. Mada, P. Lysyansky, A. M. Daraban, J. Duchenne, J.-U. Voigt, How to define end-diastole and end-systole? impact of timing on strain measurements, *JACC: Cardiovascular Imaging* 8 (2015) 148–157.

[17] F. T. Dezaki, Z. Liao, C. Luong, H. Girgis, N. Dhungel, A. H. Abdi, D. Behnami, K. Gin, R. Rohling, P. Abolmaesumi, et al., Cardiac phase detection in echocardiograms with densely gated recurrent neural networks and global extrema loss, *IEEE transactions on medical imaging* 38 (2018) 1821–1832.

[18] E. S. Lane, N. Azarmehr, J. Jevsikov, J. P. Howard, M. J. Shun-Shin, G. D. Cole, D. P. Francis, M. Zolgharni, Multibeat echocardiographic phase detection using deep neural networks, *Computers in Biology and Medicine* 133 (2021) 104373.

[19] Y. Li, H. Li, F. Wu, J. Luo, Semi-supervised learning improves the performance of cardiac event detection in echocardiography, *Ultrasonics* 134 (2023) 107058.

[20] B. Pu, N. Zhu, K. Li, S. Li, Fetal cardiac cycle detection in multi-resource echocardiograms using hybrid classification framework, *Future Generation Computer Systems* 115 (2021) 825–836.

[21] B. Pu, K. Li, J. Chen, Y. Lu, Q. Zeng, J. Yang, S. Li, Hfscd: a hybrid neural network for fetal standard cardiac cycle detection in ultrasound videos, *IEEE Journal of Biomedical and Health Informatics* (2024).

[22] L. H. Lee, J. A. Noble, Automatic determination of the fetal cardiac cycle in ultrasound using spatio-temporal neural networks, in: 2020 IEEE 17th international symposium on biomedical imaging (ISBI), IEEE, 2020, pp. 1937–1940.

[23] G. Balaji, R. Venkatesan, Optimized pyramidal convolution shuffle attention neural network based fetal cardiac cycle detection from echocardiograms, *Biomedical Signal Processing and Control* 98 (2024) 106701.

[24] Y. Lu, G. Tan, B. Pu, P.-H. Yeung, H. Wang, S. Li, J. C. Rajapakse, K. Li, Optical flow-enhanced mamba u-net for cardiac phase detection in ultrasound videos, *IEEE Transactions on Medical Imaging* (2025).

[25] P. Gifani, H. Behnam, A. Shalbaf, Z. A. Sani, Automatic detection of end-diastole and end-systole from echocardiography images using manifold learning, *Physiological measurement* 31 (2010) 1091.

[26] A. Shalbaf, Z. AlizadehSani, H. Behnam, Echocardiography without electrocardiogram using nonlinear dimensionality reduction methods, *Journal of Medical Ultrasonics* 42 (2015) 137–149.

[27] Z. Bu, Y. Liu, J. Huo, J. Peng, K. Wang, G. Zhou, R. Sparks, P. Dasgupta, A. Granados, S. Ourselin, Ddsb: An unsupervised and training-free method for phase detection in echocardiography, in: X. Xu, Z. Cui, I. Rekik, X. Ouyang, K. Sun (Eds.), *Machine Learning in Medical Imaging*, Springer Nature Switzerland, Cham, 2025, pp. 42–51.

[28] M. Sjoerdsma, S. Bouwmeester, F. van Heesch, P. Houthuizen, R. Lopata, Spatio-temporal registration of multi-perspective 3d echocardiography for improved strain estimation, *Medical Image Analysis* (2025) 103791.

[29] Y. Yang, Q. Yang, K. Cui, C. Peng, E. D’Alberti, N. Hernandez-Cruz, O. Patey, A. T. Papa-georghiou, J. A. Noble, Latent motion profiling for annotation-free cardiac phase detection in adult and fetal echocardiography videos, *arXiv preprint arXiv:2507.05154* (2025).

[30] H. Reynaud, A. Vlontzos, B. Hou, A. Beqiri, P. Leeson, B. Kainz, Ultrasound video transformers for cardiac ejection fraction estimation, in: *Medical Image Computing and Computer Assisted Intervention–MICCAI 2021: 24th International Conference, Strasbourg, France, September 27–October 1, 2021, Proceedings, Part VI 24*, Springer, 2021, pp. 495–505.

[31] Y. Zeng, P.-H. Tsui, K. Pang, G. Bin, J. Li, K. Lv, X. Wu, S. Wu, Z. Zhou, Maef-net: Multi-attention efficient feature fusion network for left ventricular segmentation and quantitative analysis in two-dimensional echocardiography, *Ultrasonics* 127 (2023) 106855.

[32] F. Laumer, G. Fringeli, A. Dubatovka, L. Manduchi, J. M. Buhmann, Deepheartbeat: Latent trajectory learning of cardiac cycles using cardiac ultrasounds, in: *Machine Learning for Health, PMLR*, 2020, pp. 194–212.

[33] W. Huang, C. P. Bridge, J. A. Noble, A. Zisserman, Temporal heartnet: towards human-level automatic analysis of fetal cardiac screening video, in: *International Conference on Medical Image Computing and Computer-Assisted Intervention*, Springer, 2017, pp. 341–349.

[34] M.-M. Rohé, M. Sermesant, X. Pennec, Low-dimensional representation of cardiac motion using barycentric subspaces: a new group-wise paradigm for estimation, analysis, and reconstruction, *Medical image analysis* 45 (2018) 1–12.

[35] K. McLeod, M. Sermesant, P. Beerbaum, X. Pennec, Spatio-temporal tensor decomposition of a polyaffine motion model for a better analysis of pathological left ventricular dynamics, *IEEE transactions on medical imaging* 34 (2015) 1562–1575.

[36] Y. Yang, M. Sermesant, Unsupervised polyaffine transformation learning for echocardiography motion estimation, in: *International Conference on Functional Imaging and Modeling of the Heart*, Springer, 2023, pp. 384–393.

[37] J. Krebs, T. Mansi, N. Ayache, H. Delingette, Probabilistic motion modeling from medical image sequences: Application to cardiac cine-mri, in: *International Workshop on Statistical Atlases and Computational Models of the Heart*, Springer, 2019, pp. 176–185.

[38] A. Siarohin, S. Lathuilière, S. Tulyakov, E. Ricci, N. Sebe, First order motion model for image animation, *Advances in neural information processing systems* 32 (2019).

[39] Y. Wang, D. Yang, F. Bremond, A. Dantcheva, Lia: Latent image animator, *IEEE Transactions on Pattern Analysis and Machine Intelligence* (2024).

[40] V. Arsigny, O. Commowick, X. Pennec, N. Ayache, A log-euclidean framework for statistics on diffeomorphisms, in: *International Conference on Medical Image Computing and Computer-Assisted Intervention*, Springer, 2006, pp. 924–931.

[41] T. Vercauteren, X. Pennec, A. Perchant, N. Ayache, Symmetric log-domain diffeomorphic registration: A demons-based approach, in: *International conference on medical image computing and computer-assisted intervention*, Springer, 2008, pp. 754–761.

[42] J. Luo, E. E. Konofagou, A fast normalized cross-correlation calculation method for motion estimation, *IEEE transactions on ultrasonics, ferroelectrics, and frequency control* 57 (2010) 1347–1357.

[43] P. Virtanen, R. Gommers, T. E. Oliphant, M. Haberland, T. Reddy, D. Cournapeau, E. Burovski, P. Peterson, W. Weckesser, J. Bright, S. J. van der Walt, M. Brett, J. Wilson, K. J. Millman, N. Mayorov, A. R. J. Nelson, E. Jones, R. Kern, E. Larson, C. J. Carey, İ. Polat,

Y. Feng, E. W. Moore, J. VanderPlas, D. Laxalde, J. Perktold, R. Cimrman, I. Henriksen, E. A. Quintero, C. R. Harris, A. M. Archibald, A. H. Ribeiro, F. Pedregosa, P. van Mulbregt, SciPy 1.0 Contributors, SciPy 1.0: Fundamental Algorithms for Scientific Computing in Python, *Nature Methods* 17 (2020) 261–272. doi:10.1038/s41592-019-0686-2.

[44] Q. Yang, K. Cui, Y. Hu, C. Peng, N. Hernandez-Cruz, R. Ahuja, E. D’Alberti, C. Raymond, O. Patey, A. Papageorgiou, et al., A deep learning framework for fetal heart tracking in ultrasound videos: Toward enhanced congenital heart defects detection, in: International Conference on Functional Imaging and Modeling of the Heart, Springer, 2025, pp. 219–230.